

## COMMUNICATION

# Crystal Structure of the GluR2 Amino-Terminal Domain Provides Insights into the Architecture and Assembly of Ionotropic Glutamate Receptors

Amber Clayton<sup>1</sup>, Christian Siebold<sup>1</sup>, Robert J. C. Gilbert<sup>1</sup>,  
Geoffrey C. Sutton<sup>1</sup>, Karl Harlos<sup>1</sup>, R. A. Jeffrey McIlhinney<sup>2</sup>,  
E. Yvonne Jones<sup>1</sup> and A. Radu Aricescu<sup>1\*</sup>

<sup>1</sup>*Division of Structural Biology, Wellcome Trust Centre for Human Genetics, University of Oxford, Roosevelt Drive, Oxford OX3 7BN, UK*

<sup>2</sup>*Anatomical Neuropharmacology Unit, Medical Research Council, Mansfield Road, Oxford OX1 3TH, UK*

Received 1 June 2009;  
received in revised form  
23 July 2009;  
accepted 28 July 2009  
Available online  
3 August 2009

Edited by R. Huber

Ionotropic glutamate receptors are functionally diverse but have a common architecture, including the 400-residue amino-terminal domain (ATD). We report a 1.8-Å resolution crystal structure of human GluR2-ATD. This dimeric structure provides a mechanism for how the ATDs can drive receptor assembly and subtype-restricted composition. Lattice contacts in a 4.1-Å resolution crystal form reveal a tetrameric (dimer-dimer) arrangement consistent with previous cellular and cryo-electron microscopic data for full-length AMPA receptors.

© 2009 Elsevier Ltd. All rights reserved.

**Keywords:** ion channel; glutamate receptor; synaptic plasticity; cell surface receptor; crystal structure

Ionotropic glutamate receptors (iGluRs) mediate the majority of excitatory synaptic neurotransmission in the central nervous system.<sup>1</sup> Fundamental synaptic plasticity events, such as long-term potentiation and depression, are consequences of iGluR signaling,<sup>1–4</sup> while dysfunctions of these receptors are linked with neurologic and neurodegenerative disorders, as well as drug addiction.<sup>1,2,5–7</sup> Vertebrate iGluRs are classified, according to their selective agonists, into three subtypes:  $\alpha$ -amino-3-hydroxy-5-methyl-4-isoxazole-propionic acid (AMPA), *N*-

methyl-D-aspartate (NMDA) and kainate.<sup>1</sup> Multiple genes (four for AMPA receptors: GluR1–GluR4; seven for NMDA: NR1, NR2A–2D, NR3A–3B; five for kainate: GluR5–GluR7 and KA1–KA2) and complex alternative splicing generate a diversity of subunits that assemble to form tetrameric receptors, with a strict subtype-restricted composition.<sup>8</sup> The extracellular region of each subunit consists of an  $\sim$ 400-residue amino-terminal domain (termed ATD), which has sequence homology with type I bacterial periplasmic binding proteins (bPBPs), and a smaller domain ( $\sim$ 250 residues) responsible for agonist binding, hence termed the ligand binding core (LBC). The LBC is assembled from two discontinuous segments, interrupted by an ion-channel domain that shows homology with the bacterial potassium channels<sup>8</sup> (Fig. 1a). Extensive structural studies of LBCs (expressed in isolation, by covalent fusion of the two segments) have revealed the mechanisms of agonist binding and receptor desensitization.<sup>8,9</sup> LBC constructs are monomeric in solution but crystallize as dimers.<sup>8</sup> Isolated ATD

\*Corresponding author. E-mail address: radu@strubi.ox.ac.uk.

Abbreviations used: GluR2, R2 subunit of ionotropic glutamate receptors (AMPA subtype); ATD, amino-terminal domain; iGluR, ionotropic glutamate receptor; AMPA,  $\alpha$ -amino-3-hydroxy-5-methyl-4-isoxazole-propionic acid; NMDA, *N*-methyl-D-aspartate; bPBP, bacterial periplasmic binding proteins; LBC, ligand binding core; HEK293S-GnTI, human embryonic kidney 293S cells, *N*-acetylglucosaminyltransferase I negative.

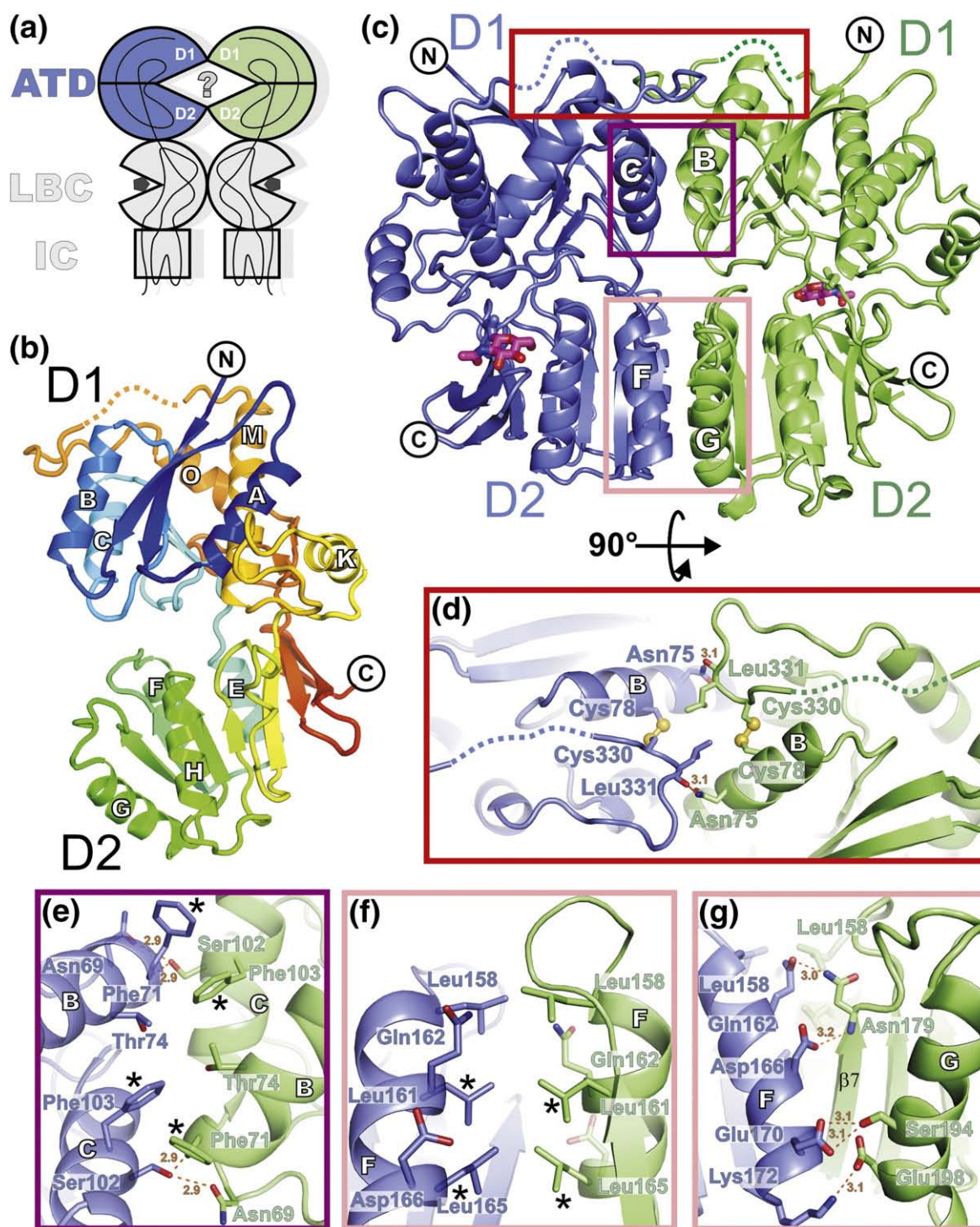


**Fig. 1.** Structure of GluR2-ATD. (a) iGluR schematic. (b) Rainbow cartoon representation of the GluR2-ATD monomer. Helices are labeled as in Supplementary Fig. 2. (c) Cartoon diagram of the GluR2-ATD dimer. The two monomers are related by a crystallographic 2-fold axis. N-linked glycans are in stick representation. (d–g) Close-up of dimer interface contacts. Dotted lines with distances show hydrogen bonds. Asterisks mark residues targeted by mutagenesis.

regions, however, dimerize in solution<sup>10–12</sup> and have been shown to control subunit dimerization and the specificity of tetrameric assembly in full-length iGluRs,<sup>13,14</sup> but their role in modulation of channel function remains obscure (in overexpression systems, ATD truncated constructs can form functional, ligand-gated, homotetrameric channels<sup>15–17</sup>). In order to gain a mechanistic understanding of ATD

functions, we undertook a structural analysis of this region from human GluR2, a subunit of crucial importance for the function of AMPA receptors.<sup>18</sup>

A construct containing GluR2 residues 25 to 412 (GluR2-ATD) was expressed in HEK293S-GnTI cells, and its structure solved at 2.5-Å resolution by selenomethionine-based single anomalous dispersion phasing (Supplementary Methods and Supplementary

**Table 1.** Crystallographic statistics

	GluR2-ATD native crystal form 1	GluR2-ATD SeMet crystal form 1	GluR2-ATD native crystal form 2
<i>Data collection</i>			
Space group	<i>I</i> 222	<i>I</i> 222	<i>P</i> 4 <sub>3</sub> 2 <sub>1</sub> 2
Cell dimensions			
<i>a</i> , <i>b</i> , <i>c</i> (Å)	51.0, 122.5, 138.9	51.2, 121.9, 138.2	224.3, 224.3 77.0
$\alpha$ , $\beta$ , $\gamma$ (°)	90, 90, 90	90, 90, 90	90, 90, 120
Resolution (Å)	50.0–1.80 (1.86–1.80)	50.0–2.45 (2.55–2.45)	50.0–4.10 (4.20–4.10)
Unique reflections	40760	16166	15949
$R_{\text{merge}}$ (%) <sup>a</sup>	8.4 (70.1)	10.8 (55.8)	12.1 (84.5)
$I/\sigma I$	23.6 (3.3)	31.1 (5.6)	23.3 (5.7)
Completeness (%)	100.0 (100.0)	98.9 (93.4)	99.6 (100.0)
Redundancy	7.5 (7.5)	20.2 (19.3)	28.5 (29.2)
<i>Refinement</i>			
Resolution (Å)	50.0–1.80 (1.86–1.80)		50.0–4.1 (4.35–4.1)
No. reflections	38999 (2981)		15433 (2260)
$R_{\text{factor}}$ (%) <sup>b</sup>	18.1 (22.2)		29.0 (31.3)
$R_{\text{free}}$ (%) <sup>c</sup>	21.7 (27.7)		35.4 (38.0)
No. atoms			
Protein	2928		8784
Sugar	14		—
Sulfate	5		—
Chloride	2		—
Acetate	4		—
Water	279		—
<i>B</i> -factors			
Protein	40		—
Sugar	43		—
Sulfate	40		—
Acetate	61		—
Water	40		—
R.m.s. deviations			
Bond lengths (Å)	0.006		0.011
Bond angles (°)	0.896		1.492

Numbers in parentheses refer to the appropriate outer shell. The asymmetric unit of crystal form 1 contains one GluR2-ATD molecule. The asymmetric unit of crystal form 2 contains three GluR2-ATD molecules.

SeMet, selenomethionine.

<sup>a</sup>  $R_{\text{merge}} = \sum_{hkl} \sum_i |I(hkl;i) - \langle I(hkl) \rangle| / \sum_{hkl} \sum_i I(hkl;i)$ , where  $I(hkl;i)$  is the intensity of an individual measurement and  $\langle I(hkl) \rangle$  is the average intensity from multiple observations.

<sup>b</sup>  $R_{\text{factor}} = \sum_{hkl} ||F_{\text{obs}}| - k|F_{\text{calc}}|| / \sum_{hkl} |F_{\text{obs}}|$

<sup>c</sup>  $R_{\text{free}}$  equals the  $R$ -factor against 5% of the data removed prior to refinement.

Fig. 1). This model was used to determine native GluR2-ATD structures at 1.8- and 4.1-Å resolution in space groups *I*222 and *P*4<sub>3</sub>2<sub>1</sub>2, respectively (Table 1). The 1.8-Å structure describes 367 residues (one molecule per crystallographic asymmetric unit, disordered residues 322–327 and 399–412 omitted). Only one of the three N-linked glycans predicted by bioinformatic analysis (using the NetNGlyc server†), trimmed down to one *N*-acetylglucosamine moiety per chain through enzymatic deglycosylation, can be clearly observed in the electron density maps following refinement (Fig. 1c). GluR2-ATD has a two-domain (D1 and D2) “flytrap” structure (Fig. 1b). Each domain has a type I bPBP  $\alpha\beta$  fold with a central  $\beta$ -sheet surrounded by  $\alpha$ -helices, similar to the leucine/isoleucine/valine binding protein (LIVBP, PDB 2LIV, 11% sequence identity, rmsd of 2.1 Å for 177 equivalent C $\alpha$  positions in D1 and 2.3 Å for 126 equivalent C $\alpha$  positions in D2) and metabotropic glutamate receptor ectodomains (e.g., mGluR1, PDB 1EWT, 12% sequence identity, rmsd of 1.9 Å for 171 equivalent C $\alpha$  positions in D1 and

2.1 Å for 147 equivalent C $\alpha$  positions in D2). To facilitate comparisons, we have adopted the mGluR1  $\alpha$ -helix nomenclature<sup>19</sup> (Supplementary Fig. 2).

GluR2-ATD is dimeric in solution (Supplementary Fig. 3a; dissociation constant of 4.3  $\mu$ M as determined by analytical ultracentrifugation) and within the crystal lattice is arranged as parallel dimers with 1400 Å<sup>2</sup> of buried surface per monomer contributed equally by D1 and D2 (Fig. 1c). The D1–D1 interface consists of 16 residues per monomer involved in van der Waals contacts that are bordered by six hydrogen bonds. Three structural elements contribute a large, apical loop (residues 318–331; Loop 1) and  $\alpha$ -helices B and C (Fig. 1d and e). Loop 1 is tethered to helix B by a disulfide bond (Cys78–Cys330) that sequence analysis indicates to be conserved in all iGluRs. The D2–D2 interface is more hydrophilic in nature, with 13 residues per monomer involved in van der Waals interactions bordered by 10 hydrogen bonds and two salt bridges. The main contributors are helix F,  $\beta$ -strand 7 and helix G (Fig. 1f and g). Sequence analysis reveals that the zipper-like arrangement, formed by three aliphatic side chains of helix F residues per monomer, is conserved in AMPA and kainate

† <http://www.cbs.dtu.dk/services/NetNGlyc/>

receptors (Supplementary Fig. 2) but absent in NMDA receptors. We carried out site-directed mutagenesis to probe the dimer interface (Fig. 1e and f). Two mutations designed to disrupt D1–D1 (either Phe71Asp or Thr74Asn/Ala76Ser, introducing an N-linked glycosylation site) abolished protein dimerization (Supplementary Fig. 3a); the remaining mutations prevented correct protein folding, blocking secretion (Supplementary Fig. 4).

In contrast to the GluR2-ATD interface, the mGluR1 ectodomain dimer (previously used for homology modeling iGluR ATDs) has a more open arrangement (Fig. 2a). The D1–D1 interface also involves the B and C helices; however, residues equivalent to Loop 1 adopt a completely different conformation, pointing away from the interface, and there are no D2–D2 contacts in either the apo- or ligand-bound structures. Overall, the mGluR1 interface is only some 65% of that in GluR2-ATD (903 Å<sup>2</sup> in PDB 1EWT). This suggests that the domains of the mGluR flytrap have a larger relative mobility, consistent with the conformational changes observed upon ligand binding.<sup>19</sup> D1-based superpositions with open and closed (ligand-bound) LIVBP structures reveal that GluR2-ATD has an intermediate degree of flytrap closure (Fig. 2b). Detailed comparison with mGluR1 is complicated by an additional twist component but also indicates that GluR2-ATD lies between the open and closed states of other flytrap structures. A fully open domain arrangement appears less likely to occur in GluR2-ATD due to the extensive D2–D2 interface.

Vertebrate AMPA sequence alignments mapped onto the GluR2-ATD surface revealed four conserved areas: Loop1, the D1 and D2 dimerization interfaces and the interdomain cleft, the site of ligand binding in bPBPs and mGluRs (Fig. 2c). The cores of the D1 and D2 interfaces remained conserved when vertebrate kainate receptors were included in the alignment (Fig. 2d), but Loop 1 and the interdomain cleft were revealed as regions of subtype specificity. This observation suggests that Loop 1 may be a crucial element in imposing the restrictions on heterodimerization between iGluR subtypes observed by Ayalon *et al.*<sup>14</sup> The striking subtype-specific conservation of the interdomain cleft raises the possibility that AMPA and kainate ATDs can bind specific ligands, as established for the NMDA receptor subunits (where the extent of ligand-induced closure correlates with channel “open probability”).<sup>20</sup> If so, the D2–D2 interface may function as a “safety catch”, stabilising the receptor ectodomain in the absence of an appropriate ligand. Following ligand binding, domain reorientation, for example to a fully closed flytrap,

could provide a mechanism to transmit structural changes to other regions of the receptor as proposed for NMDA receptors.<sup>20,21</sup> The interdomain cleft has a positive electrostatic potential resulting from AMPA subtype-specific arginines (Supplementary Fig. 5). B-factor analysis and inspection of the electron density maps reveal a high degree of flexibility in the D2 residues contributing to the cleft (Supplementary Fig. 6).

Multi-angle light-scattering experiments revealed a concentration-dependent tendency of GluR2-ATD to form a higher oligomeric form, most likely tetrameric (Supplementary Fig. 3a). Analytical ultracentrifugation experiments confirmed the presence of GluR2-ATD tetramers in solution (Fig. 3a), with a dimer–tetramer dissociation constant of 50 μM (Supplementary Methods). Our 4.1-Å resolution crystal form contains a crystallographic and a noncrystallographic dimer, both identical with the 1.8-Å dimer structure. These two dimers lie parallel with each other in the crystal lattice and make a symmetric dimer–dimer contact through D2 (Fig. 3b). This putative tetramerization surface is contributed to by helix H and the subsequent loop plus the β9–β10 loop, a region that shows clear evidence of flexibility in the 1.8-Å crystal structure. Cellular experiments have previously suggested a role for D2 in modulating the iGluR tetrameric assembly.<sup>14</sup> The 4.1-Å tetrameric arrangement is reminiscent of that observed in crystals of the structurally homologous natriuretic peptide receptor ectodomain (PDB 1DP4, 1JDN, 1JDP) and could be fitted into previously reported cryo-negative electron microscopy density maps of full-length AMPA receptors isolated from a native source (rat brain)<sup>22,23</sup> without changing the relative orientation of the dimers (Fig. 3c). The closer packing of GluR2-ATD dimers suggested by alternative single particle reconstructions of recombinant AMPA receptors purified from insect cells<sup>24,25</sup> was not observed in our crystal forms.

The crystal structures of rat GluR6-ATD and rat GluR2-ATD were reported while this manuscript was in preparation.<sup>26,27</sup> Although the overall architecture of the ATDs is conserved, and consistent with the one described here for the human GluR2-ATD, GluR6 (a kainate receptor subunit) and GluR2 are functionally different.<sup>1,4,13,14</sup> This is reflected in multiple subtype-specific structural elements, such as Loop 1 and the interdomain cleft. In addition, the degree of the ATD flytrap closure also differs: the GluR6-ATD is more open (by 7° and 11°, respectively, in two crystal forms),<sup>27</sup> supporting our hypothesis that conformational rearrangements of the ATD are possible. It is also interesting to note the significant differences in the oligomerisation

**Fig. 2.** Specificity determinants in iGluR ATDs. (a) Solvent accessible surface representation of GluR2-ATD and mGluR1-flytrap (PDB 1EWT) dimers. The D1 domains of the left-hand-side molecules are structurally aligned. (b) Flytrap closure in GluR2-ATD (slate) compared with the open (red, PDB 2LIV) and closed (yellow, PDB 1Z16) conformations of LIVBP. All structures are superposed on D1. Values indicate maximal rotation angles of D2 relative to D1. (c and d) Sequence conservation of ATDs from vertebrate AMPA receptors (c) and vertebrate AMPA plus kainate receptors (d) mapped on the GluR2-ATD structure. Circles highlight the interdomain cleft, ellipses Loop 1 and rectangles the dimerization interfaces of D1 and D2.

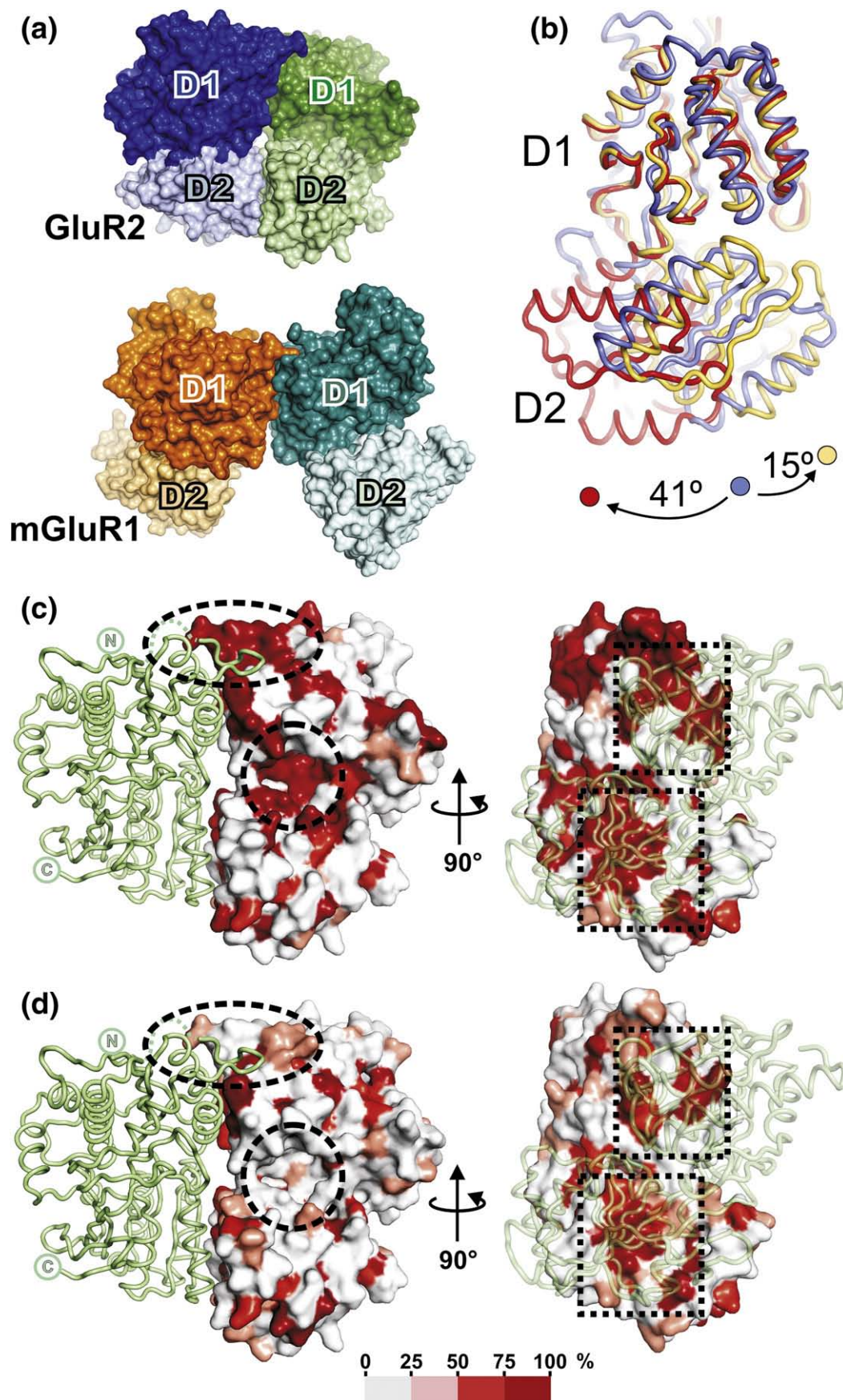
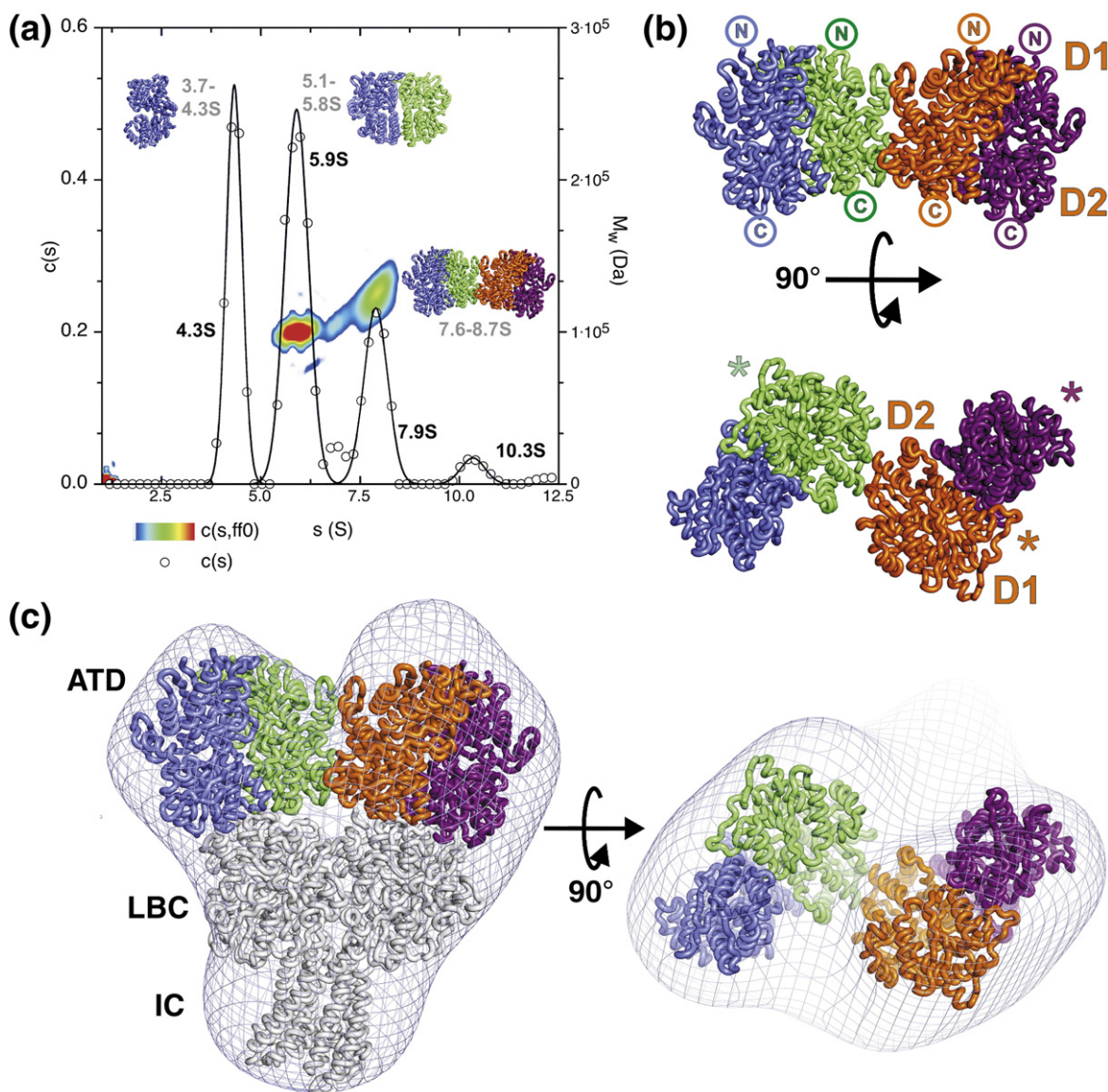


Fig. 2 (legend on previous page)



**Fig. 3.** A putative tetrameric arrangement of ATDs in AMPA receptors. (a) Analytical ultracentrifugation (sedimentation velocity) of GluR2-ATD at 0.6 mg/ml. The contour plot shows only the nontrivial peaks for molecular weights ( $y$ -axis) of sedimenting species ( $x$ -axis). The sedimentation coefficient of each species is shown in black type, derived from a Gaussian fit of the peak. Calculated sedimentation coefficients are shown in grey. (b) Cartoon representation of the tetrameric arrangement in the 4.1-Å GluR2-ATD structure. Asterisks indicate the molecules in the crystallographic asymmetric unit. (c) Manual fit of the tetramer in cryo-electron microscopy density map of native AMPA receptors.<sup>22</sup> The GluR2-LBC (PDB 1LBC) and an ion-channel model based on the transmembrane segment of KcsA (PDB 1BL8) are depicted in grey.

properties of rat *versus* human GluR2-ATDs in solution. The large difference in the calculated dimer dissociation constants (4.3  $\mu$ M reported here *versus* 152 nM reported by Jin *et al.*<sup>26</sup>) may result from the different approaches used in the processing of analytical ultracentrifugation data (we calculated  $K_d$  values in a model-independent way, allowing for the formation of higher oligomers). The dimerization  $K_d$  value calculated by Kumar *et al.* for the related GluR6-ATD<sup>27</sup> (15  $\mu$ M) is similar to the one reported here. Interestingly, the presence of tetramers in solution, described here for the human GluR2-ATD expressed in human cells, with wild-type glycosylation, was not observed in rat GluR2-

ATD (produced in insect cells).<sup>26</sup> It is unclear whether the different structure of glycans underlies the observed differences (insect cell glycans are typically truncated to  $\text{Man}_3\text{GlcNAc}_2$ ) and this remains to be investigated by future studies.

In summary, the GluR2-ATD structures described here provide insights into fundamental aspects of iGluR assembly and highlight several avenues for future research. These include the analysis of potential ligand (small- or macro-molecular) binding to the interdomain clefts of AMPA and kainate receptor ATDs and validation of the observed tetrameric arrangement of ATDs within the context of full-length AMPA receptors. Furthermore, the

GluR2-ATD region is responsible for the induction of dendritic spines in hippocampal neurons,<sup>28</sup> a function most likely mediated by its ability to interact (in *cis* or *trans*) with other cell surface molecules such as N-cadherin<sup>29</sup> and/or the neuronal pentraxins.<sup>30,31</sup> Structural investigations of these complexes will bring a new dimension to the understanding of GluR2 biology.

### Protein Data Bank accession numbers

Atomic coordinates and structure factors of GluR2-ATD have been deposited at the Protein Data Bank with accession numbers 2wjw (crystal form 1) and 2wjx (crystal form 2).

### Acknowledgements

We thank the staff of European Synchrotron Radiation Facility beamlines BM14, ID29, and ID23-EH2 for assistance with data collection; T. Walter for help with crystallization; M. Mayer, S. Graham and D. Stuart for advice and discussion; and T. Nakagawa and T. Walz for providing electron microscopy density maps. We acknowledge the use of the crystallization facilities provided by the MRC-funded Oxford Protein Production Facility. The work was funded by the UK Medical Research Council. C.S. is a Wellcome Trust Career Development Fellow. R.J.C.G. is a Royal Society University Research Fellow. E.Y.J. is a CR-UK Principal Research Fellow. A.R.A. is an MRC Career Development Fellow.

A.C. and A.R.A. produced the constructs and crystallized the proteins. K.H., C.S. and A.R.A. collected X-ray data, C.S. and A.R.A. processed X-ray data and solved the structures. R.J.C.G. performed the AUC experiments. G.S. performed the MALS experiments. All authors contributed to data analysis and interpretation. C.S., E.Y.J. and A.R.A. wrote the paper. A.R.A. designed and supervised this project.

### Supplementary Data

Supplementary data associated with this article can be found, in the online version, at [doi:10.1016/j.jmb.2009.07.082](https://doi.org/10.1016/j.jmb.2009.07.082)

### References

- Dingledine, R., Borges, K., Bowie, D. & Traynelis, S. F. (1999). The glutamate receptor ion channels. *Pharmacol. Rev.* **51**, 7–61.
- Cull-Candy, S., Kelly, L. & Farrant, M. (2006). Regulation of Ca<sup>2+</sup>-permeable AMPA receptors: synaptic plasticity and beyond. *Curr. Opin. Neurobiol.* **16**, 288–297.
- Malinow, R. & Malenka, R. C. (2002). AMPA receptor trafficking and synaptic plasticity. *Annu. Rev. Neurosci.* **25**, 103–126.
- Madden, D. R. (2002). The structure and function of glutamate receptor ion channels. *Nat. Rev. Neurosci.* **3**, 91–101.
- Kemp, J. A. & McKernan, R. M. (2002). NMDA receptor pathways as drug targets. *Nat. Neurosci.* **5**, 1039–1042.
- Conrad, K. L., Tseng, K. Y., Uejima, J. L., Reimers, J. M., Heng, L. J., Shaham, Y. *et al.* (2008). Formation of accumbens GluR2-lacking AMPA receptors mediates incubation of cocaine craving. *Nature*, **454**, 118–121.
- Van den Oever, M. C., Goriounova, N. A., Li, K. W., Van der Schors, R. C., Binnekade, R., Schoffelmeer, A. N. *et al.* (2008). Prefrontal cortex AMPA receptor plasticity is crucial for cue-induced relapse to heroin-seeking. *Nat. Neurosci.* **11**, 1053–1058.
- Mayer, M. L. (2006). Glutamate receptors at atomic resolution. *Nature*, **440**, 456–462.
- Sun, Y., Olson, R., Horning, M., Armstrong, N., Mayer, M. & Gouaux, E. (2002). Mechanism of glutamate receptor desensitization. *Nature*, **417**, 245–253.
- Kuusinen, A., Abele, R., Madden, D. R. & Keinänen, K. (1999). Oligomerization and ligand-binding properties of the ectodomain of the  $\alpha$ -amino-3-hydroxy-5-methyl-4-isoxazole propionic acid receptor subunit GluRD. *J. Biol. Chem.* **274**, 28937–28943.
- Meddows, E., Le Bourdelles, B., Grimwood, S., Wafford, K., Sandhu, S., Whiting, P. & McIlhinney, R. A. (2001). Identification of molecular determinants that are important in the assembly of N-methyl-D-aspartate receptors. *J. Biol. Chem.* **276**, 18795–18803.
- Wells, G. B., Lin, L., Jeanlos, E. M. & Anand, R. (2001). Assembly and ligand binding properties of the water-soluble extracellular domains of the glutamate receptor 1 subunit. *J. Biol. Chem.* **276**, 3031–3036.
- Ayalon, G., Segev, E., Elgavish, S. & Stern-Bach, Y. (2005). Two regions in the N-terminal domain of ionotropic glutamate receptor 3 form the subunit oligomerization interfaces that control subtype-specific receptor assembly. *J. Biol. Chem.* **280**, 15053–15060.
- Ayalon, G. & Stern-Bach, Y. (2001). Functional assembly of AMPA and kainate receptors is mediated by several discrete protein–protein interactions. *Neuron*, **31**, 103–113.
- Horning, M. S. & Mayer, M. L. (2004). Regulation of AMPA receptor gating by ligand binding core dimers. *Neuron*, **41**, 379–388.
- Matsuda, S., Kamiya, Y. & Yuzaki, M. (2005). Roles of the N-terminal domain on the function and quaternary structure of the ionotropic glutamate receptor. *J. Biol. Chem.* **280**, 20021–20029.
- Pasternack, A., Coleman, S. K., Jouppila, A., Mottershead, D. G., Lindfors, M., Pasternack, M. & Keinänen, K. (2002).  $\alpha$ -Amino-3-hydroxy-5-methyl-4-isoxazolepropionic acid (AMPA) receptor channels lacking the N-terminal domain. *J. Biol. Chem.* **277**, 49662–49667.
- Isaac, J. T., Ashby, M. & McBain, C. J. (2007). The role of the GluR2 subunit in AMPA receptor function and synaptic plasticity. *Neuron*, **54**, 859–871.
- Kunishima, N., Shimada, Y., Tsuji, Y., Sato, T., Yamamoto, M., Kumasaka, T. *et al.* (2000). Structural basis of glutamate recognition by a dimeric metabotropic glutamate receptor. *Nature*, **407**, 971–977.
- Gielen, M., Retchless, B. S., Mony, L., Johnson, J. W. & Paoletti, P. (2009). Mechanism of differential control of NMDA receptor activity by NR2 subunits. *Nature*, **459**, 703–707.
- Zheng, F., Erreger, K., Low, C. M., Banke, T., Lee, C. J., Conn, P. J. & Traynelis, S. F. (2001). Allosteric

- interaction between the amino terminal domain and the ligand binding domain of NR2A. *Nat. Neurosci.* **4**, 894–901.
22. Nakagawa, T., Cheng, Y., Sheng, M. & Walz, T. (2006). Three-dimensional structure of an AMPA receptor without associated stargazin/TARP proteins. *Biol. Chem.* **387**, 179–187.
  23. Nakagawa, T., Cheng, Y., Ramm, E., Sheng, M. & Walz, T. (2005). Structure and different conformational states of native AMPA receptor complexes. *Nature*, **433**, 545–549.
  24. Midgett, C. R. & Madden, D. R. (2008). The quaternary structure of a calcium-permeable AMPA receptor: conservation of shape and symmetry across functionally distinct subunit assemblies. *J. Mol. Biol.* **382**, 578–584.
  25. Tichelaar, W., Safferling, M., Keinänen, K., Stark, H. & Madden, D. R. (2004). The three-dimensional structure of an ionotropic glutamate receptor reveals a dimer-of-dimers assembly. *J. Mol. Biol.* **344**, 435–442.
  26. Jin, R., Singh, S. K., Gu, S., Furukawa, H., Sobolevsky, A. I., Zhou, J. *et al.* (2009). Crystal structure and association behaviour of the GluR2 amino-terminal domain. *EMBO J.* **28**, 1812–1823.
  27. Kumar, J., Schuck, P., Jin, R. & Mayer, M. L. (2009). The N-terminal domain of GluR6-subtype glutamate receptor ion channels. *Nat. Struct. Mol. Biol.* **16**, 631–638.
  28. Passafaro, M., Nakagawa, T., Sala, C. & Sheng, M. (2003). Induction of dendritic spines by an extracellular domain of AMPA receptor subunit GluR2. *Nature*, **424**, 677–681.
  29. Saglietti, L., Dequidt, C., Kamieniarz, K., Rousset, M. C., Valnegri, P., Thoumine, O. *et al.* (2007). Extracellular interactions between GluR2 and N-7cadherin in spine regulation. *Neuron*, **54**, 461–477.
  30. O'Brien, R. J., Xu, D., Petralia, R. S., Steward, O., Huganir, R. L. & Worley, P. (1999). Synaptic clustering of AMPA receptors by the extracellular immediate-early gene product Narp. *Neuron*, **23**, 309–323.
  31. Sia, G. M., Beique, J. C., Rumbaugh, G., Cho, R., Worley, P. F. & Huganir, R. L. (2007). Interaction of the N-terminal domain of the AMPA receptor GluR4 subunit with the neuronal pentraxin NP1 mediates GluR4 synaptic recruitment. *Neuron*, **55**, 87–102.